Plant Nano Biology 13 (2025) 100188

Contents lists available at ScienceDirect

Plant Nano Biology

journal homepage: www.journals.elsevier.com/plant-nano-biology

Different types of honey on the synthesis of silver nanoparticles (AgNPs) and their antibacterial activity: In-vitro and in-silico studies

Saidun Fiddaroini [a], Kurnia Indu [a], Luailik Madaniyah [a], Suci Amalia [b], Aulanni'am [a], Moh. Farid Rahman [a], Akhmad Sabarudin [a,*]

[a] Department of Chemistry, Faculty of Science, Brawijaya University, Malang, Indonesia
[b] Chemistry Study Program, Faculty of Science and Technology, Maulana Malik Ibrahim Islamic State University, Malang, Indonesia

ARTICLE INFO

Keywords:
AgNPs
Nanoparticles
Honey
Reducing sugar
Antibacterial activity

ABSTRACT

AgNPs exhibit significant antibacterial activity, which is enhanced by their nanoscale size. Green synthesis using honey offers an eco-friendly, straightforward approach, with glucose and fructose in honey playing key roles in AgNPs synthesis. This study explores the effects of glucose and fructose concentrations in various honey types on AgNPs formation at 27–30 °C and pH 6–6.5, complemented by molecular docking studies. The sugar content in different honey samples was as follows: Cottonwood (56.66 %), Rambutan (49.95 %), Rubber (44.54 %), and Coffee (37.56 %). Higher bioreductor concentrations led to increased absorbance in the UV-Vis spectra; however, antibacterial activity decreased, albeit not significantly. This can be attributed to lower reducing sugar concentrations, which resulted in smaller AgNPs with a larger surface area, consequently affecting their antibacterial efficacy. The synthesized AgNPs were spherical (8–10 nm) and exhibited face-centered cubic crystallinity. The inhibition zones for AgNPs derived from cottonwood, rambutan, rubber, and coffee honey against *Staphylococcus aureus* were 14.51 mm, 14.54 mm, 15.45 mm, and 16.04 mm, respectively, and against *Pseudomonas aeruginosa* were 15.10 mm, 15.70 mm, 15.81 mm, and 15.90 mm, respectively. The microdilution broth assay revealed a sharp increase in antibacterial inhibition within the AgNPs concentration range of 5–50 ppm, plateauing above 50 ppm, with the steep increase halting between 20 and 40 ppm. MIC values ranged from 11.47 to 13.37 ppm for *S. aureus* and 8.71–10.62 ppm for *P. aeruginosa*. Molecular docking studies confirmed that D-glucose and D-fructose bind to bacterial proteins PBP2a and PBP3, supporting their role as bioreductors in AgNPs formation.

1. Introduction

AgNPs are silver particles ranging from 1 to 100 nm in size, exhibiting unique properties due to their nanoscale dimensions (Asif et al., 2022; Galatage et al., 2021). AgNPs can be synthesized through various methods, including chemical, physical, and biological approaches, which primarily rely on reduction processes using chemical agents or biological organisms to produce nanosized silver particles (Dhaka et al., 2023). Renowned for their potent antimicrobial activity (Lee and Jun, 2019), AgNPs have been extensively utilized in diverse applications, such as antimicrobial coatings (Amr et al., 2023) and water treatment systems (Tiwari et al., 2023). In medicine, AgNPs are crucial for producing antimicrobial bandages, manufacturing medical devices, and supporting wound healing (Krishnan et al., 2020; Yudaev et al., 2022).

AgNPs have long been recognized as potent antibacterial agents due to their remarkable potential across various applications (Huq and Akter, 2021; Khan et al., 2019). Their antibacterial efficacy is primarily attributed to their nanoscale size, which provides a high surface area and enhanced biological activity (Long et al., 2022). The minute dimensions of AgNPs enable their penetration through bacterial cell membranes, allowing direct interaction with intracellular components (More et al., 2023; Qing et al., 2018). Once inside, AgNPs can bind to bacterial DNA (Mikhailova, 2020), leading to structural damage, inhibition of replication, and suppression of bacterial growth (Ahmad et al., 2020). Additionally, AgNPs disrupt bacterial metabolic processes by inhibiting key enzymes essential for survival (Kusi et al., 2020). Another critical mechanism involves interference with the bacterial respiratory system, which impairs energy production and ultimately results in cell death (Qing et al., 2018).

Various approaches have been established for synthesizing silver nanoparticles (AgNPs) with tailored sizes and morphologies. Chemical synthesis typically employs reductants such as sodium borohydride

* Corresponding author.
E-mail address: sabarjpn@ub.ac.id (A. Sabarudin).

https://doi.org/10.1016/j.plana.2025.100188
Received 13 September 2024; Received in revised form 7 February 2025; Accepted 1 September 2025
Available online 2 September 2025

(Mavani and Shah, 2013) or citrate (Jassim et al., 2022) to reduce silver ions into nanoparticles. Physical methods, like laser ablation, utilize laser irradiation on silver powder to generate AgNPs (Mamdouh et al., 2022). In contrast, biological or "green" synthesis leverages plant extracts and microorganisms as natural bioreductants for nanoparticle formation (Huq et al., 2022). Among these techniques, biological synthesis stands out for its environmental sustainability, high biocompatibility, and superior control over particle size. Furthermore, it offers enhanced safety, excellent stability, full biodegradability, and a straightforward bioprocess, making it a promising method for producing AgNPs (Madaniyah et al., 2025a; Rai et al., 2021).

The use of honey as a bioreductor in AgNPs synthesis highlights an innovative application of biological methodologies for nanoparticle production (Fiddaroini et al., 2025). Bioreductor serve as reducing agents that convert silver ions into nanoparticles (Fiddaroini et al., 2023; Naganthran et al., 2022). Honey, a complex matrix rich in polyphenols, flavonoids, and sugars, functions effectively as a natural redox agent during the synthesis process (Cianciosi et al., 2018; Olas, 2020). The biocompatible nature of honey's constituents enhances the environmental and health-related attributes of AgNPs synthesized via this approach, offering an eco-friendly alternative to conventional chemical methods (Keskin et al., 2023). Moreover, the physicochemical properties of the resulting AgNPs—such as size, shape, and distribution—are strongly influenced by the chemical composition of the honey and the synthesis parameters employed.

The composition and concentration of compounds in honey are critical determinants of the physicochemical properties of AgNPs synthesized using this approach (Strapasson et al., 2023). The concentration of bioreductants significantly impacts the reduction kinetics and particle growth, with higher bioreductant levels often resulting in larger nanoparticles (Samuel et al., 2022; Sun et al., 2019). Additionally, the particle size distribution and morphology are influenced by the bioreductant concentration (Zhang et al., 2021). This parameter also affects the optical properties of the AgNPs, including their coloration, which varies with particle size, distribution, and the presence of specific compounds capable of modulating light absorption or scattering at particular wavelengths (Asif et al., 2022).

This study aims to quantify the concentration of reducing sugars in various types of honey and evaluate their influence on the synthesis, characterization, and phytochemical properties of AgNPs, as well as their antibacterial activity. The investigation focuses on the effects of varying reducing sugar concentrations on the synthesis process, including the mechanisms of AgNP formation and reactivity. Additionally, the study analyzes the physicochemical characteristics of AgNPs synthesized using honey as a bioreductor. Antibacterial activity is assessed through in-vitro testing, complemented by an in-silico evaluation of the synergistic effects of honey components in AgNP synthesis.

2. Methods

2.1 Materials and instrumentation

This study utilized four types of honey as bioreductants: coffee (*Coffea spp*.) honey, cottonwood (*Ceiba pentandra*) honey, rambutan (*Nephelium lappaceum*) honey, and rubber (*Hevea brasiliensis*) honey, sourced from Agro Tawon-Rimba Raya Farms, Bedali, Lawang District, Malang Regency, East Java. The precursors employed included silver nitrate ($AgNO_3$, EMSURE 99 %), D-glucose (anhydrous, Merck), D-fructose (powder, Merck), anthrone reagent, and distilled water. Test microorganisms comprised *Staphylococcus aureus* (ATCC 25922, Gram-positive) and *Pseudomonas aeruginosa* (ATCC 9027, Gram-negative). Additional materials included infusion solution (0.9 % NaCl), nutrient agar (Merck), Mueller hinton broth, barium chloride ($BaCl_2$, Sigma-Aldrich), and sulfuric acid (98 % EMSURE).

Characterization of the synthesized AgNPs was performed using a range of advanced instruments, including an Ultraviolet-Visible Spectrophotometer (UV-Vis Model 1601, Shimadzu, Japan), Fourier Transform Infrared Spectroscopy (FTIR Shimadzu IR-Tracer 100, Japan), Transmission Electron Microscope (TEM, Hitachi TM 3000), X-Ray Diffraction (XRD, PANalytical, Japan), Scanning Electron Microscope (SEM, Hitachi FLEXSEM 100) and Energy-Dispersive X-ray Spectroscopy (EDX, FEI Quanta FEG 650).

2.2 Preparation of glucose and fructose standard curves

The glucose and fructose content in honey samples was quantified using the anthrone method. Standard calibration curves for glucose and fructose were constructed by preparing standard solutions at concentrations of 0, 20, 40, 60, 80, and 100 ppm in 5 mL volumes. To each solution, 2 mL of anthrone reagent was added. The anthrone reagent was prepared by dissolving 0.1 g of anthrone in concentrated H_2SO_4. The mixtures were then heated at 80 °C for 20 min, resulting in a bluish-green coloration. Absorbance of the solutions was measured using a UV-Vis spectrophotometer, and standard curves were generated by plotting absorbance against concentration. Linear regression equations were derived from the plotted data.

2.3 Analysis of reducing sugar content in honey

A 0.5 mL aliquot of the honey sample was accurately measured and dissolved in 100 mL of distilled water. From this solution, 5 mL was transferred into a test tube, and 2 mL of anthrone reagent was added. The mixture was heated at 80 °C for 20 min to induce the development of a bluish-green color. The absorbance of the resulting solution was measured using a UV-Vis spectrophotometer. The reducing sugar concentration was determined by correlating the measured absorbance to the standard calibration curves for glucose and fructose.

2.4 Synthesis of AgNPs

The synthesis of AgNPs was carried out by adding 3 % honey extract-which served as the bioreductor-to 0.1 M silver nitrate ($AgNO_3$) as the precursor in the ratio of 1:1 (v/v). The reaction mixture, under stirring using a magnetic stirrer (200–300 rpm) at room temperature (27–30 °C) for 10 min, was well mixed. The solution was, therefore, exposed to a halogen lamp for about 30 min. This was the period that the formation of silver nanoparticles, as evidenced by the color change of the solution to brown, occurred.

2.5 Characterization of AgNPs

2.5.1 UV-Vis spectroscopy

UV-Vis spectroscopy was employed to analyze reducing sugar content using the anthrone method and to evaluate the formation of AgNPs synthesized with honey as a bioreductor. Measurements were performed using a UV-Vis spectrophotometer across a wavelength range of 200–800 nm. The glucose and fructose content in honey was determined by comparing the absorbance values to standard spectra of glucose and fructose. For AgNPs, UV-Vis analysis was conducted to confirm nanoparticle formation post-reaction. Samples were placed in a 1 cm quartz cuvette for analysis. The formation of AgNPs was verified by the presence of absorbance peaks within the 400–450 nm range, indicative of surface plasmon resonance (SPR), thus confirming successful nanoparticle synthesis.

2.5.2 Fourier transform infra-red

Infrared (IR) radiation enables the analysis of molecular absorption and transmission properties, producing a distinctive spectrum for each molecule, akin to a molecular fingerprint. In this study, Fourier Transform Infrared (FTIR) spectroscopy was utilized to characterize honey as a bioreductant and the synthesized AgNPs. Measurements were conducted at room temperature over the wavelength range of

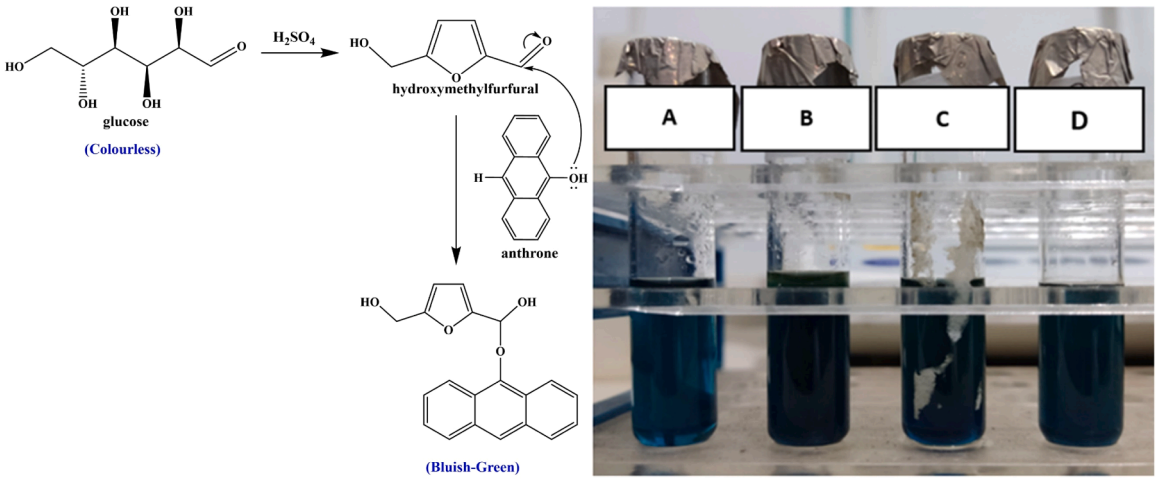

Fig. 1. Reaction mechanism of glucose detection by anthrone method (left) and honey solution (coffee (a); rubber (b); rambutan (c); cottonwood (d)) mixed with anthrone reagent (right).

400–4000 cm^{-1} . AgNP samples were freeze-dried prior to FTIR analysis to ensure a high concentration of nanoparticles, while honey samples were analyzed without any additional preparation or dilution.

2.5.3 X-ray diffraction

XRD analysis confirmed the crystallinity and estimated the particle size of AgNPs synthesized using honey as a bioreductant. Measurements were performed with a CuKα radiation source (λ = 1.5418 Å) at a 2°/min scanning rate over a 2θ range of 10°–80°. Diffraction peaks matched JCPDS database references, confirming the crystalline structure. The Scherrer equation was used to estimate particle size from the FWHM of the peaks.

2.5.4 Morphology analysis with SEM and TEM

The surface morphology and elemental composition of AgNPs synthesized using honey as a bioreductant were analyzed using SEM combined with EDX. Dried and colloidal AgNP samples were mounted on aluminum stubs and coated with a thin carbon layer to enhance conductivity. Imaging was conducted at an accelerating voltage of 10 kV, providing high-resolution SEM images to evaluate particle size, shape, and distribution. Simultaneously, EDX analysis was performed on colloidal AgNPs to confirm the elemental composition and verify the presence of silver. This combined analysis also offered insights into surface roughness and morphology at the micrometer scale.

TEM analysis provided morphological and structural characterization of AgNPs. Samples were dispersed in water, deposited on carbon-coated copper grids, and dried. Imaging at ≥ 100 kV enabled precise size measurement, shape assessment, and crystalline structure verification. ImageJ software was used for particle size distribution analysis.

2.6 In-vitro antibacterial activity test

2.6.1 Agar well diffusion method

The antibacterial activity of AgNPs synthesized using various bioreductors—coffee, cottonwood, rambutan, and rubber—was evaluated against *S. aureus* (Gram-positive) and *P. aeruginosa* (Gram-negative) using the agar well diffusion method. Nutrient agar (NA) was prepared by dissolving 20 g/L in distilled water, followed by boiling. The medium and associated equipment were sterilized via autoclaving at 121 °C and 15 psi for 15 min. After sterilization, the agar was cooled to 45 °C. Bacterial suspensions were standardized to a McFarland 0.5 turbidity equivalent in 0.9 % NaCl.

Approximately 15 mL of agar was poured into sterile Petri dishes, and 100 μL of bacterial suspension was evenly spread across the solidified medium. Wells with a diameter of 6 mm were created in the agar, and 20 μL of each AgNP sample prepared with honey bioreductants was introduced into the wells. Plates were incubated at 37 °C for 24 h. Antibacterial activity was determined by measuring the diameter of the inhibition zones in horizontal, vertical, and diagonal orientations using calipers. Each experiment was performed in triplicate to ensure reproducibility.

2.6.2. Broth microdilution assay

The nutrient broth (medium) was prepared by dissolving 2.1 g of Mueller-Hinton Broth (MHB) powder in 100 mL of distilled water, followed by homogenization and sterilization at 121 °C for 15 min. After cooling at room temperature (27–30 °C), the medium was used for bacterial suspension preparation. *S. aureus* and *P. aeruginosa* stored in slant cultures were revived by streaking onto the nutrient broth and incubated at 37 °C for 24 h. A single colony from the cultured bacteria was then suspended in the medium. The bacterial cell density was adjusted to McFarland standard 0.5 (~10^6 CFU/mL) using serial dilution in the medium if necessary.

AgNPs samples synthesized from different honey bioreductors (coffee, cottonwood, rambutan, and rubber) were prepared at varying concentrations (300, 150, 75, 37.5, 18.75, 9.375, and 4.69 ppm). A 100 μL aliquot of each sample was added to a 96-well plate, followed by triplicate testing for each condition. Subsequently, 100 μL of *S. aureus* and *P. aeruginosa* suspension was introduced into each well. The positive control consisted of bacterial cultures without AgNP treatment, while the negative control contained only the growth medium. The plate was then incubated at 37 °C for 24 h. Absorbance was measured using an ELISA reader, and the percentage of inhibition (Eq. 1) was calculated for each sample to determine the minimum inhibitory concentration (MIC) required for 50 % bacterial growth inhibition of AgNPs synthesized from various honey bioreductors.

$$\%\text{Inhibition} = \frac{A\ (positive\ control) - A\ (sample)}{A\ (positive\ control)} \times 100\% \quad (1)$$

Note: A (positive control): absorbance of bacterial culture without AgNP treatment

A (sample): absorbance of the sample containing AgNPs

2.7 In-Silico study and antibacterial evaluation

Molecular docking studies were conducted in silico to investigate the binding interactions and mechanisms of honey-derived phytochemicals with target proteins of *S. aureus* and *P. aeruginosa*. The target proteins included penicillin-binding proteins (PBPs), which play a key role in bacterial cell wall synthesis and are primary targets of beta-lactam

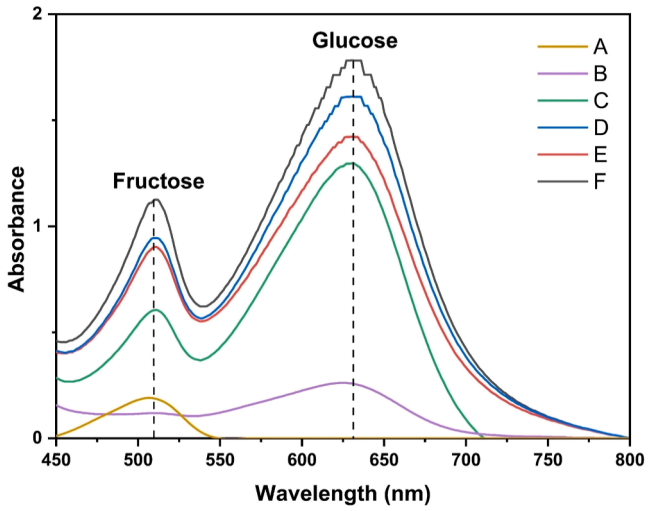

Fig. 2. Analytical results from the UV-Vis instrument for 20 ppm fructose standard (a), 20 ppm glucose standard (b), 0.5 % coffee honey (c), 0.5 % rambutan honey (d), 0.5 % rubber honey (e), and 0.5 % cottonwood honey (f).

antibiotics. Crystal structures of the proteins were obtained from the RCSB Protein Data Bank (PDB) (https://www.rcsb.org/) using PDB IDs: PBP2a and PBP3.

Honey phytochemicals, such as D-glucose and D-fructose, were selected based on their known composition in honey. Molecular formulas and weights of the ligands were retrieved from PubChem, and their 2D structures were generated using OpenBabel in PyRx. The ligands were prepared for docking, and simulations were performed using AutoDock Vina with default settings in PyRx, adjusting the grid box parameters to target the active sites of the proteins.

Binding affinities and ligand poses were analyzed post-docking, with the best conformations selected for detailed evaluation. The interactions, including hydrogen bonding, van der Waals forces, and other critical molecular interactions, were visualized using Discovery Studio. These analyses provided insights into the potential of the selected phytochemicals as antibacterial agents against the target bacterial species.

3. Results and discussion

3.1 Determining the reducing sugar content in various types of honey

The reducing sugar content of different honey types was quantified using the anthrone method. The analysis involved an initial reaction with concentrated sulfuric acid at 5 °C, which facilitated the generation of hydroxymethylfurfural (HMF) and produced a yellow-colored solution. Subsequent addition of anthrone reagent and heating at 80 °C resulted in the formation of a blue-green HMF-anthrone complex. This colorimetric change, measured via UV-Vis spectrophotometry, enabled the quantification of reducing sugars, specifically glucose and fructose, in the honey samples (Fig. 1). Glucose and fructose concentrations were determined based on their respective absorbance maxima at 627 nm and 510 nm (Fig. 2). Calibration curves were constructed to correlate absorbance values with reducing sugar concentrations (Fig. 3).

The reducing sugar content, expressed as a percentage, varied significantly among the honey types tested. Cottonwood honey exhibited the highest reducing sugar content (56.66 %), followed by rambutan honey (49.95 %), rubber honey (44.54 %), and coffee honey (37.56 %) (Table 1). These variations highlight the influence of botanical origin on the chemical composition of honey. The differences in reducing sugar content can be attributed to the unique nectar sources associated with each plant species, which impact the biochemical pathways of sugar synthesis and breakdown during nectar formation.

Cottonwood (*C. pentandra*) nectar is characterized by a higher proportion of sugars that are readily hydrolyzed into glucose and fructose, aligning with its elevated reducing sugar content. In contrast, nectar from rambutan (*N. lappaceum*), rubber (*H. brasiliensis*), and coffee (*Coffea spp.*) plants contains relatively higher sucrose levels and lower concentrations of reducing sugars. This variation reflects the distinct metabolic pathways and enzymatic activities specific to each plant species, as well as genetic and environmental factors influencing nectar composition (Nepi et al., 2018; Nicolson, 2022).

Furthermore, the observed differences in reducing sugar content may also result from geographical and climatic variations, which affect the phenotypic expression of plants and subsequently alter their nectar profiles (Samuel et al., 2022). For instance, factors such as soil composition, temperature, and humidity have been shown to impact the synthesis and accumulation of sugars within plant nectaries. Therefore, the sugar composition of honey is not only a reflection of plant taxonomy but also an integration of environmental influences on nectar production.

Table 1
Calculation of total bioreductor content in each honey.

Honey Type	Fructose Content (%)	Glucose Content (%)	Total bioreductor content (%)
Cottonwood	12.49	44.17	56.66
Rambutan	10.23	39.72	49.95
Rubber	9.72	34.82	44.54
Coffee	6.01	31.55	37.56

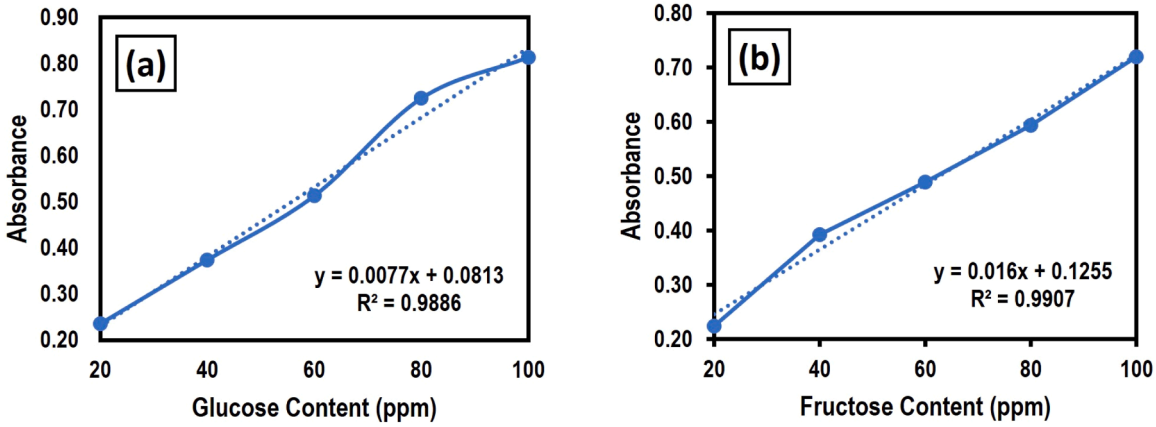

Fig. 3. Standard curves of Glucose (a) and Fructose (b).

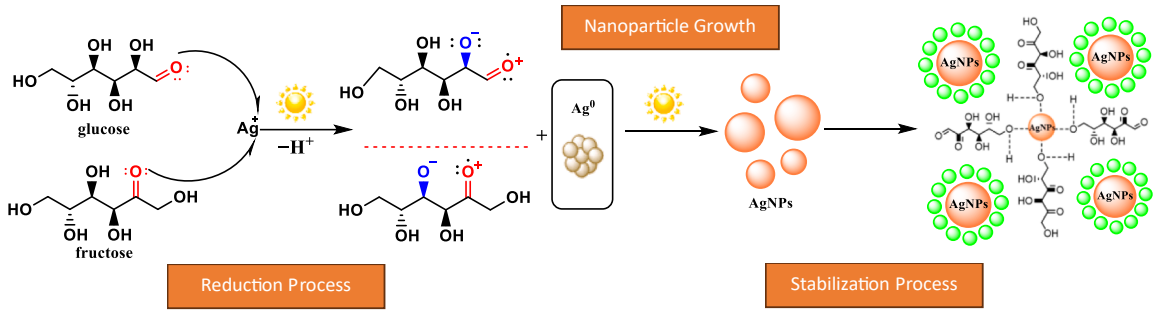

Fig. 4. Formation mechanism of AgNPs.

This analysis underscores the pivotal role of reducing sugars as bioreductor in honey-mediated AgNP synthesis. The higher reducing sugar content in cottonwood honey suggests its superior potential for nanoparticle synthesis due to enhanced reduction kinetics and particle formation efficiency. This aligns with previous studies emphasizing the significance of sugar composition in optimizing green synthesis protocols for nanomaterials (Keskin et al., 2023). However, AgNPs synthesized with a high bioreductant concentration may exhibit larger particle sizes, as accelerated reaction kinetics during nanoparticle formation can promote rapid particle growth and potential aggregation.

3.2 Effect of reducing sugar content on the AgNPs synthesis

The synthesis of AgNPs was achieved using a biological approach, employing honey-derived reducing agents. The process involved the irradiation of honey with halogen lamps, which activated carbonyl groups in glucose and fructose. This activation generated reactive H^* ions capable of reducing Ag^+ ions into neutral silver atoms, facilitating the formation of AgNPs (Fig. 4). While both glucose and fructose serve as monosaccharide-based reducing agents, their reduction efficiencies differ significantly. Glucose, with its reactive aldehyde group, exhibits a notably higher reduction rate compared to fructose (Yahia et al., 2019). Fructose, possessing a ketone group, lacks the same direct reducing capability and must undergo isomerization to glucose to enhance its reductive activity (Semchyshyn et al., 2014). Consequently, glucose generally facilitates faster reduction, although the reaction efficiency can vary depending on specific reaction conditions.

Upon the formation of silver atoms, the nucleation process was initiated, wherein a limited number of silver atoms aggregated to establish a stable nucleus. This nucleus served as a foundational site for the subsequent growth of nanoparticles. During the growth phase, newly reduced silver atoms continued to deposit onto the nucleus, resulting in the formation of larger silver nanoparticles (Thanh et al., 2014). The growth of AgNPs synthesized using honey-derived bioreductors occurs after nucleation and proceeds through two primary mechanisms. The first mechanism, diffusion-limited growth, involves the diffusion of silver atoms to the nanoparticle surface, where they adhere and accumulate in successive layers. The rate of this growth is modulated by factors such as the concentration of silver ions, ambient temperature, and the viscosity of the honey solution (Yang, 2021).

The second mechanism, Ostwald ripening, entails the dissolution of smaller nanoparticles, with silver atoms from these particles migrating to larger, thermodynamically more stable nanoparticles (Alarcon et al., 2023). This phenomenon results in the generation of nanoparticles with larger sizes and narrower size distributions. Active components within honey, including reducing sugars (glucose and fructose) and polyphenols, play a critical role during this phase by acting as capping agents. These compounds stabilize the nanoparticle surfaces, mitigating excessive aggregation and ensuring particle uniformity. The formation of a protective molecular layer around the AgNPs helps maintain their size and prevents coalescence, thereby enhancing the stability and functionality of the nanoparticles.

The synthesized AgNPs were characterized using UV-Vis spectroscopy, revealing a maximum absorbance peak at 445 nm, confirming the presence of AgNPs (Fig. 5). The intensity of absorbance corresponded to the color density of the AgNPs solution, with higher values indicating darker solutions and larger particle sizes. AgNPs synthesized with cottonwood honey exhibited the highest absorbance (0.426), followed

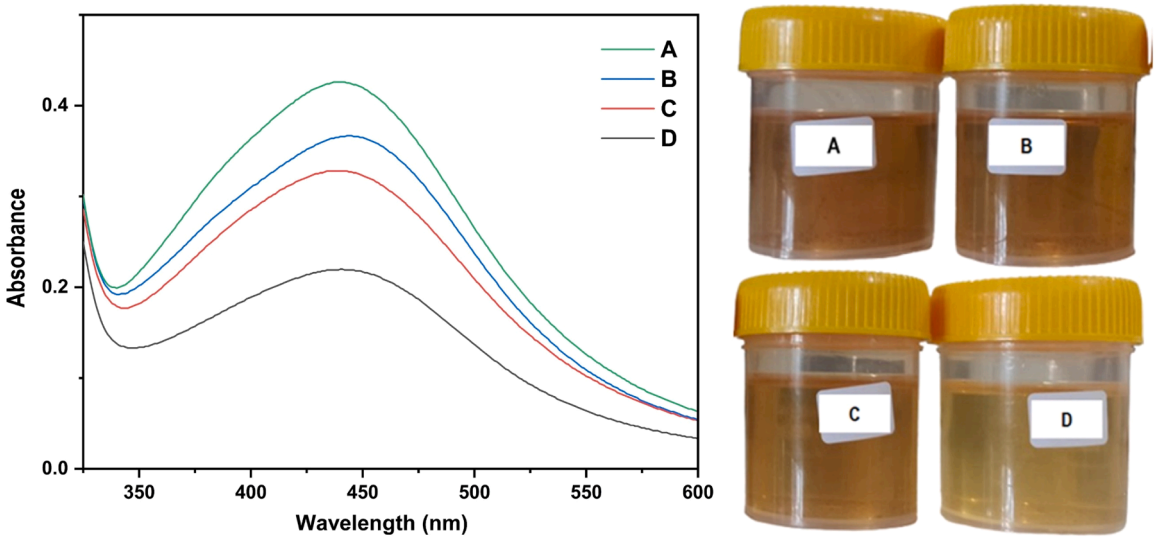

Fig. 5. UV-Vis spectra of AgNPs reduced with various bioreductors of cottonwood (a), rambutan (b), rubber (c) and coffee (d) honeys.

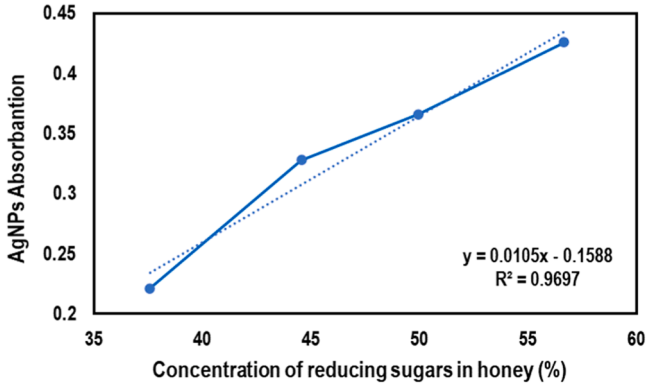

Fig. 6. The relationship between reducing sugar concentration and the absorbance of the resulting AgNPs.

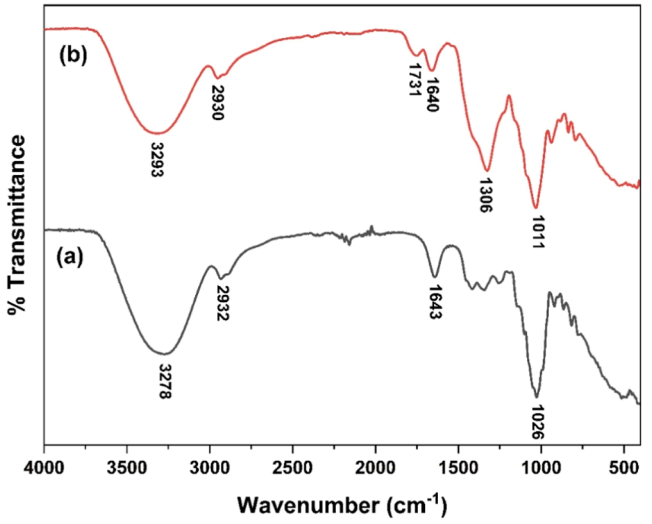

Fig. 7. The FTIR Analysis of Cottonwood Honey (a) and AgNPs with Cottonwood Honey Bioreductor (b).

by rambutan (0.366), rubber (0.328), and coffee honey (0.221).

Differences in absorbance among the honey types are attributable to variations in bioreductant concentrations, such as reducing sugars (Indana et al., 2016; Kumar et al., 2020; Qaeed et al., 2023). A broader absorption spectrum observed for cottonwood honey-derived AgNPs indicates a wider particle size distribution, while the narrower peaks for coffee honey suggest smaller, more uniform nanoparticles (Zielińska et al., 2009). These findings underscore the influence of reducing sugar concentrations, with higher levels promoting increased reduction rates and larger particle formation.

Studies confirm that lower concentrations of bioreductants lead to reduced absorbance (Fig. 6) and lighter solution coloration, which are indicative of smaller nanoparticle sizes (Alharbi et al., 2022; De Leersnyder et al., 2019). A lower availability of bioreductors increases the spatial volume within the solution, reducing particle interactions and aggregation, thus promoting the formation of smaller nanoparticles. (Gudkov et al., 2020).

3.3 Characterization of AgNPs

The FTIR analysis of AgNPs synthesized using cottonwood honey and pure cottonwood honey show on Fig. 7 reveals several absorption bands indicating the presence of specific functional groups. One of the primary absorption bands, with high intensity and broadening at 3293 cm^{-1} (AgNPs) dan 3278 cm^{-1} (cottonwood honey), indicates the

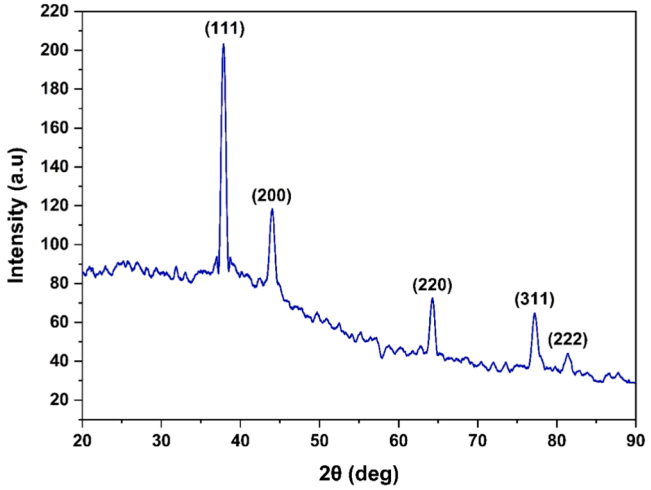

Fig. 8. The X-ray diffraction (XRD) diffractogram of silver nanoparticles (AgNPs) reduced by cottonwood honey.

presence of hydroxyl (O-H) groups, likely originating from phenolic compounds, flavonoids, or proteins in honey, which may be adsorbed on the surface of the AgNPs. This also includes glucose and fructose, which are the main bioreductants in the synthesis of AgNPs contained in honey. Additionally, a low-intensity absorption band observed around 2930 cm^{-1} (AgNPs) dan 2932 cm^{-1} (cottonwood honey) can be associated with C-H bonds from organic compounds in honey. A shift in the peak observed for cottonwood honey at a wavenumber of 1643 cm^{-1} was noted, which changed to two overlapping peaks at 1640 cm^{-1} and 1731 cm^{-1} in the AgNPs sample. This shift indicates a modification in spectral characteristics, with the region representing the carbonyl (C═O) groups from aldehyde (glucose) and ketone (fructose) functional groups. This characteristic shift suggests that the formation of AgNPs occurs via electron donation from these carbonyl groups. This phenomenon is illustrated in Fig. 4.

A notable difference is observed at a wavenumber of 1306 cm^{-1} in the AgNPs spectrum, whereas a similar peak with the same intensity is absent in the cottonwood honey sample. This area can be interpreted in two ways: as a C-O (stretching) vibration from carboxyl or alcohol groups, or as a C-H (bending) vibration from organic components such as carbohydrates or phenolic compounds. In this context, the high-intensity absorption at 1306 cm^{-1} in the AgNPs sample is likely attributed to organic components in cottonwood honey that act as stabilizers or capping agents on the AgNPs surface, helping to prevent aggregation and providing stability to the nanoparticles. These findings support the argument that these functional groups serve as natural stabilizers in the AgNPs reduced from cottonwood honey, as illustrated in Fig. 4.

The peak at 1026 cm^{-1} in cottonwood honey shifts to 1011 cm^{-1} in AgNPs, indicating the presence of functional groups associated with the vibration of hydroxyl (-OH) groups or C-O bonds, typically observed in the range of 1000–1300 cm^{-1} . In the context of honey as a bioreductor, this peak is likely related to C-O vibrations from sugars or other organic compounds present in honey, such as polysaccharides or phenolic compounds. This functional group may also suggest the presence of glycosidic structures or vibrations from ester or ether groups found in honey components involved in the formation of AgNPs. Overall, this FTIR spectrum reveals the presence of various functional groups from organic compounds in honey that interact with the surface of the AgNPs. These interactions likely play a crucial role in the stabilization of the nanoparticles and may influence the physicochemical properties and biological activity of the synthesized AgNPs.

XRD analysis of AgNPs synthesized with cottonwood honey as a bioreductor (Fig. 8) revealed diffraction peaks at 2θ values of 37.91°, 44.14°, 64.29°, 77.12°, and 81.38°, corresponding to the (111), (200),

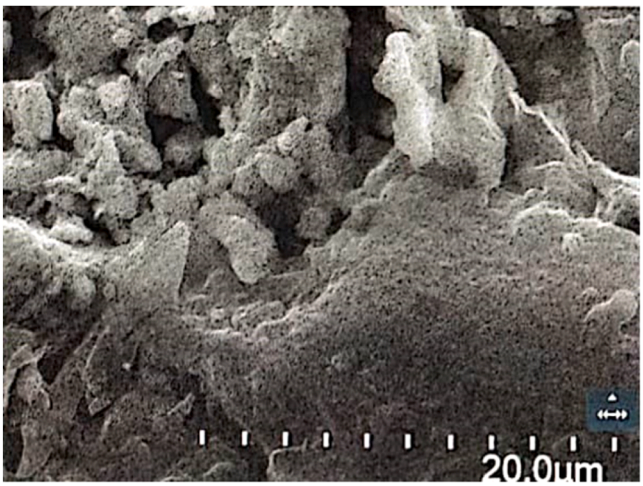

Fig. 9. SEM Analysis of Dried AgNPs at 20,000x Magnification.

(220), (311), and (222) planes of the FCC silver structure (JCPDS file 04–0783). These results confirm that the synthesized AgNPs exhibit a typical FCC silver crystal structure. The Debye-Scherrer equation was applied to estimate the crystal size using the most prominent peak at $2\theta = 37.91°$, representing the (111) plane. This peak, characterized by its sharpness and intensity, provides reliable data for size estimation, as it is less affected by impurities. With an FWHM value of 0.1673, the estimated crystal size of AgNPs synthesized with cottonwood honey was approximately 50.22 nm.

The morphological analysis of AgNPs was conducted using SEM on samples synthesized with cottonwood honey as a bioreductor (Fig. 9) to obtain detailed surface characterization. The samples tested were freeze-dried, resulting in the compression of AgNPs into a high-concentration matrix. The results show that the surface appears rough with the presence of nanoparticle aggregation, which is not evenly distributed. The complex texture and uneven surface indicate particle agglomeration, which often occurs in nanoparticles due to van der Waals forces or inter-particle interactions. These interactions cause small particles to merge into larger structures, reducing the individual distribution of single particles.

The results from the FESEM-EDX analysis of colloidal AgNPs reduced using cottonwood honey are shown in Fig. 10. Fig. 10**a** displays the FESEM micrograph, revealing the overall morphology of the colloidal AgNPs. The surface appears aggregated and highly dense, which is characteristic of biologically synthesized nanoparticles. The nanoparticles appear as a cluster of varying sizes, suggesting effective reduction and stabilization by honey compounds.

Moreover, the SEM image of the colloidal AgNPs (Fig. 10) is noticeably clearer compared to dried AgNPs (Fig. 9), which tend to appear clumped and less defined. This indicates that the colloidal form preserves the nanoparticle structure more effectively, preventing excessive aggregation. The superior clarity of the colloidal AgNPs further highlights their enhanced stability in liquid suspension, which is critical for maintaining their biological activity. Colloidal AgNPs offer better storage stability, minimizing aggregation and preserving their functional properties over time, whereas dried AgNPs are prone to loss of stability and reduced bioactivity due to the clumping effect. This reinforces the importance of storing AgNPs in colloidal form to ensure sustained biological efficacy, particularly in applications such as antimicrobial and therapeutic treatments (Madaniyah et al., 2025b).

Fig. 10**b** shows the EDX spectrum, which confirms the presence of silver as the primary elemental component. The prominent Ag peak is observed, indicating successful formation of AgNPs. Other elements detected include nitrogen (N), oxygen (O), and carbon (C), which can be attributed to organic molecules from honey capping and stabilizing the AgNPs. The EDX quantitative analysis shows that the elemental composition consists of N (18.08 %), O (14.53 %), C (35.61 %), and Ag (31.77 %). The substantial presence of C and O suggests that the organic components of honey, such as sugars and proteins, are effectively capping the nanoparticles, providing stability to the colloidal solution. The nitrogen content may arise from amino acids or proteins present in the honey.

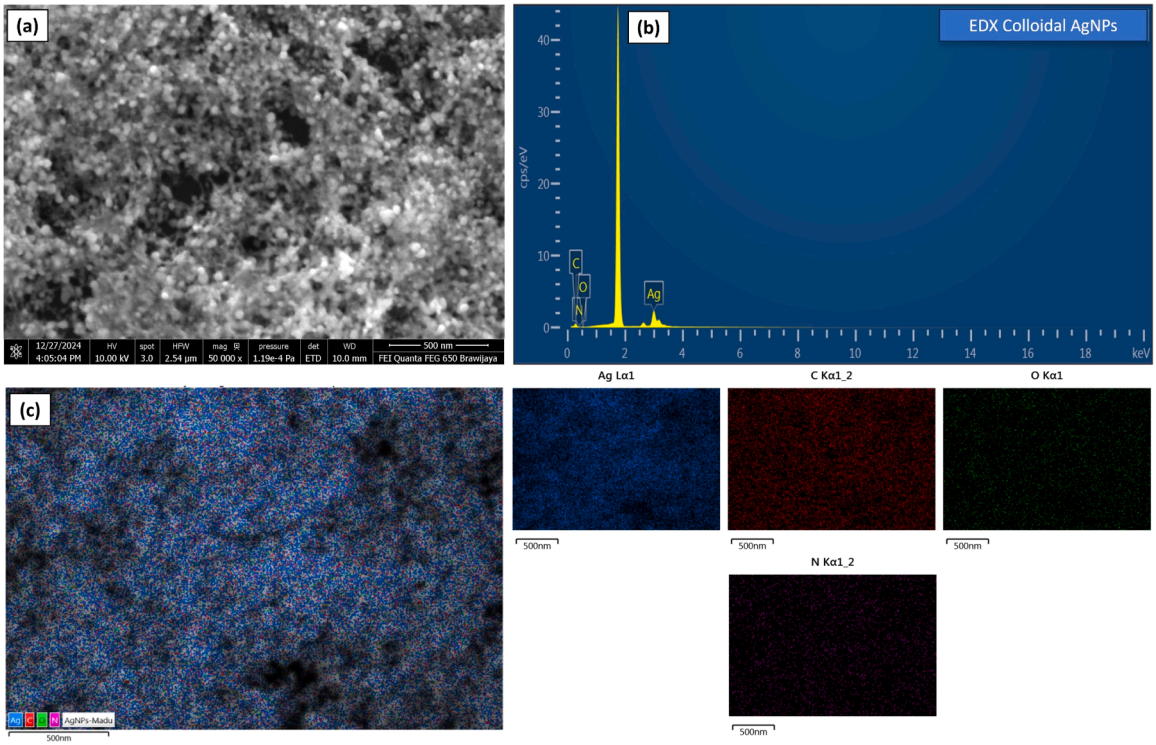

Fig. 10. FESEM image at 50,000 × magnification (a), EDX Spectra (b), and EDX mapping (c) of colloidal AgNPs with cottonwood honey bioreductor.

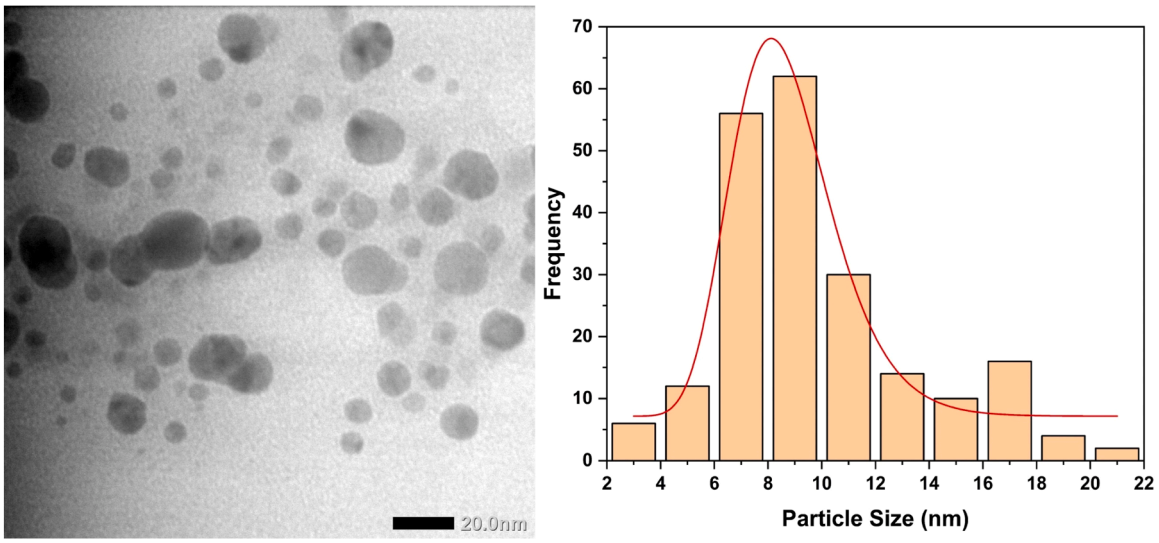

Fig. 11. TEM analysis results of colloidal AgNPs at 100,000× magnification.

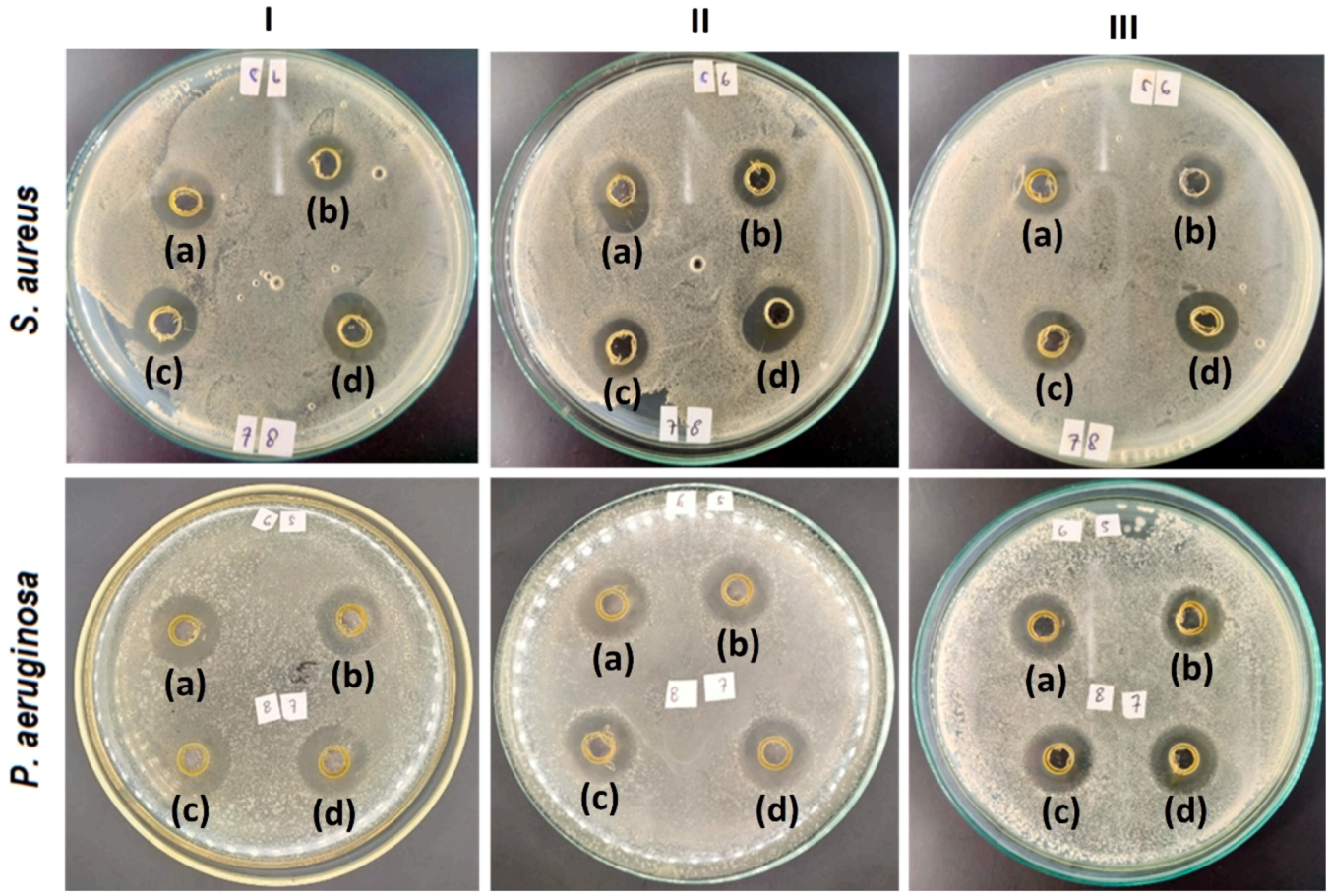

Fig. 12. Antibacterial activity test against Gram-positive (*S. aureus*) and Gram-negative bacteria (*P. aeruginosa*) of AgNPs with bioreductor of cottonwood honey (a), rambutan honey (b), rubber honey (c), and coffee honey (d). All test were repeated 3 times.

Fig. 10**c** illustrates the elemental mapping images, further confirming the uniform distribution of Ag along with C, O, and N throughout the sample. The silver nanoparticles are homogeneously dispersed, indicating efficient reduction and stabilization processes during synthesis. These results highlight that honey serves as both a reducing and stabilizing agent in the green synthesis of AgNPs, with the organic constituents providing a biocompatible coating that ensures stability and prevents aggregation. The high silver content, combined with significant amounts of carbon, nitrogen, and oxygen, suggests the successful formation of biofunctionalized AgNPs with potential applications in antimicrobial and therapeutic domains.

Based on the TEM results of AgNP colloids synthesized using

Table 2
Inhibition zone data of antibacterial activity of AgNPs against gram-positive and negative bacteria (n = 3).

AgNPs with variation in bioreductors (types of Honey)	Inhibition zones (mm)	
	S. aureus	*P. aeruginosa*
Cottonwood	14.52 ± 0.36	15.10 ± 0.99
Rambutan	14.54 ± 0.37	15.70 ± 0.51
Rubber	15.47 ± 0.36	15.81 ± 0.75
Coffee	16.04 ± 0.53	15.90 ± 0.38

cottonwood honey as a bioreductor (Fig. 11), the AgNPs exhibit an imperfect spherical shape with smooth surfaces. The particle sizes range from 2 to 22 nm, with an average particle size of 9.85 nm, and the highest frequency observed in the 8–10 nm size range. The particle size distribution indicates a tendency towards polydispersity, as the particles are not entirely uniform in size. This non-uniformity is attributed to the aggregation of some particles before achieving stability through the natural compounds present in the honey bioreductor.

3.4 In-vitro antibacterial activity test

The antibacterial activity of silver nanoparticles (AgNPs) synthesized from various honey types was evaluated through inhibition zone measurements (Fig. 12). The results revealed inhibition zones for AgNPs derived from cottonwood, rambutan, rubber, and coffee honey against Gram-positive bacteria *S. aureus* as 14.51 mm, 14.54 mm, 15.45 mm, and 16.04 mm, respectively, and against Gram-negative bacteria *P. aeruginosa* as 15.10 mm, 15.70 mm, 15.81 mm, and 15.90 mm, respectively (Table 2).

The antibacterial activity results obtained from the microdilution broth assay in Fig. 13 reveal that for all honey variations, the antibacterial effect (% inhibition) sharply increases within the AgNP concentration range of 5–50 ppm. However, at concentrations above 50 ppm, the rise in antibacterial activity becomes less significant, eventually plateauing. According to the graph in Fig. 13, the concentration range of 20–40 ppm marks the point where the steep increase in antibacterial activity halts for both *S. aureus* and *P. aeruginosa*. Beyond this point, the inhibition rate begins to plateau, indicating that further increases in AgNP concentration no longer contribute significantly to enhanced antibacterial activity. This suggests that a bactericidal saturation point has been reached, where most of the viable bacterial cells have been sufficiently inhibited, and additional AgNPs fail to improve the inhibitory effect.

The MIC (Table 3) represents the lowest concentration of AgNPs required to inhibit of 50 % bacterial growth effectively. In this study, MIC calculations were conducted at AgNPs concentrations of 4.69, 9.37, and 18.75 ppm, as these concentrations showed a clear, measurable increase in antibacterial activity on the inhibition curve. For *S. aureus*, the MIC values for AgNPs synthesized using different honey types were as follows: Cottonwood (13.37 ppm), Rambutan (12.54 ppm), Rubber (12.26 ppm), and Coffee (11.47 ppm), with Coffee honey demonstrating the highest antibacterial effectiveness due to its lowest MIC value. Similarly, for *P. aeruginosa*, the MIC values were Cottonwood (10.62 ppm), Rambutan (10.32 ppm), Rubber (9.39 ppm), and Coffee (8.71 ppm). The data show that AgNPs synthesized using Coffee honey exhibited the strongest antibacterial activity. These results suggest that Coffee honey-reduced AgNPs are the most potent against both bacterial strains, likely due to the unique bioreductant properties of Coffee honey, which enhance the efficiency of nanoparticle synthesis and its subsequent antibacterial effect.

Table 3
Minimum inhibitory concentration of AgNPs with honey variations as bioreductor.

Bioreductor of AgNPs (Honey Variation)	Minimum Inhibitory Concentration (ppm)	
	S. aureus	*P. aeruginosa*
Cottonwood	13.37	10.62
Rambutan	12.54	10.32
Rubber	12.26	9.39
Coffee	11.47	8.71

Table 4
Studies on the effect of AgNPs size on antibacterial activity.

Reductor	Particle Size (nm)	Inhibition Zones (mm)		Ref
		S. aureus	*P. aeruginosa*	
Honey	9.85	14.52 ± 0.36	15.10 ± 0.99	This work
Aloe vera	18.5	14.3 ± 0.6	13.1 ± 0.4	(Al-mehdhar et al., 2024)
Syzygium polyanthum	27.69	13.00 ± 1.32	12.00 ± 0.50	(Khan et al., 2023)
trisodium citrate*	52	slight	slight	(Iwuji et al., 2024)
Arthrospira platensis	58.68	10 ± 0.2	8.9 ± 0.1	(Obaid et al., 2024)
Lactobacillus salivarius	79.47	~7.5	~8.5	(Abdelgadir et al., 2024)

Note: Synthesis by chemical method (*)

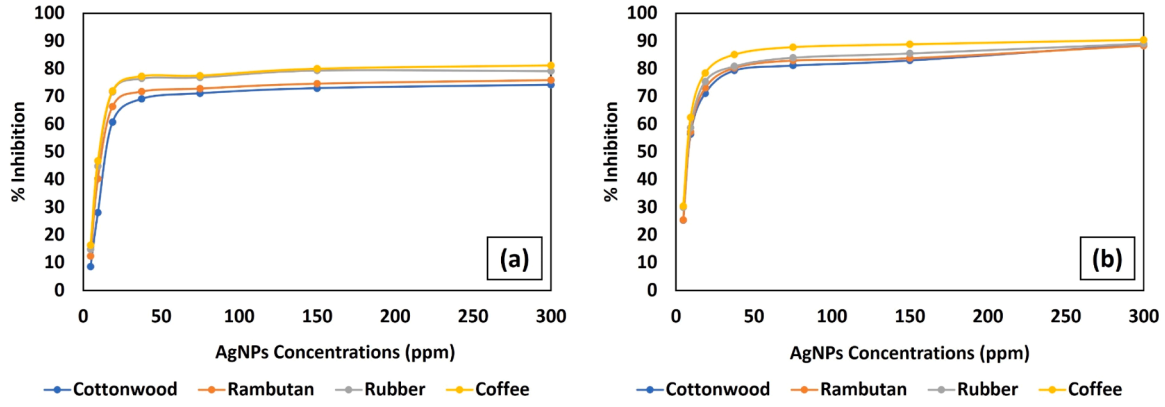

Fig. 13. Antibacterial activity of AgNPs synthesized using different honey types (Cottonwood, Rambutan, Rubber, and Coffee) against *S. aureus* (a) and *P. aeruginosa* (b) assessed via microdilution broth assays.

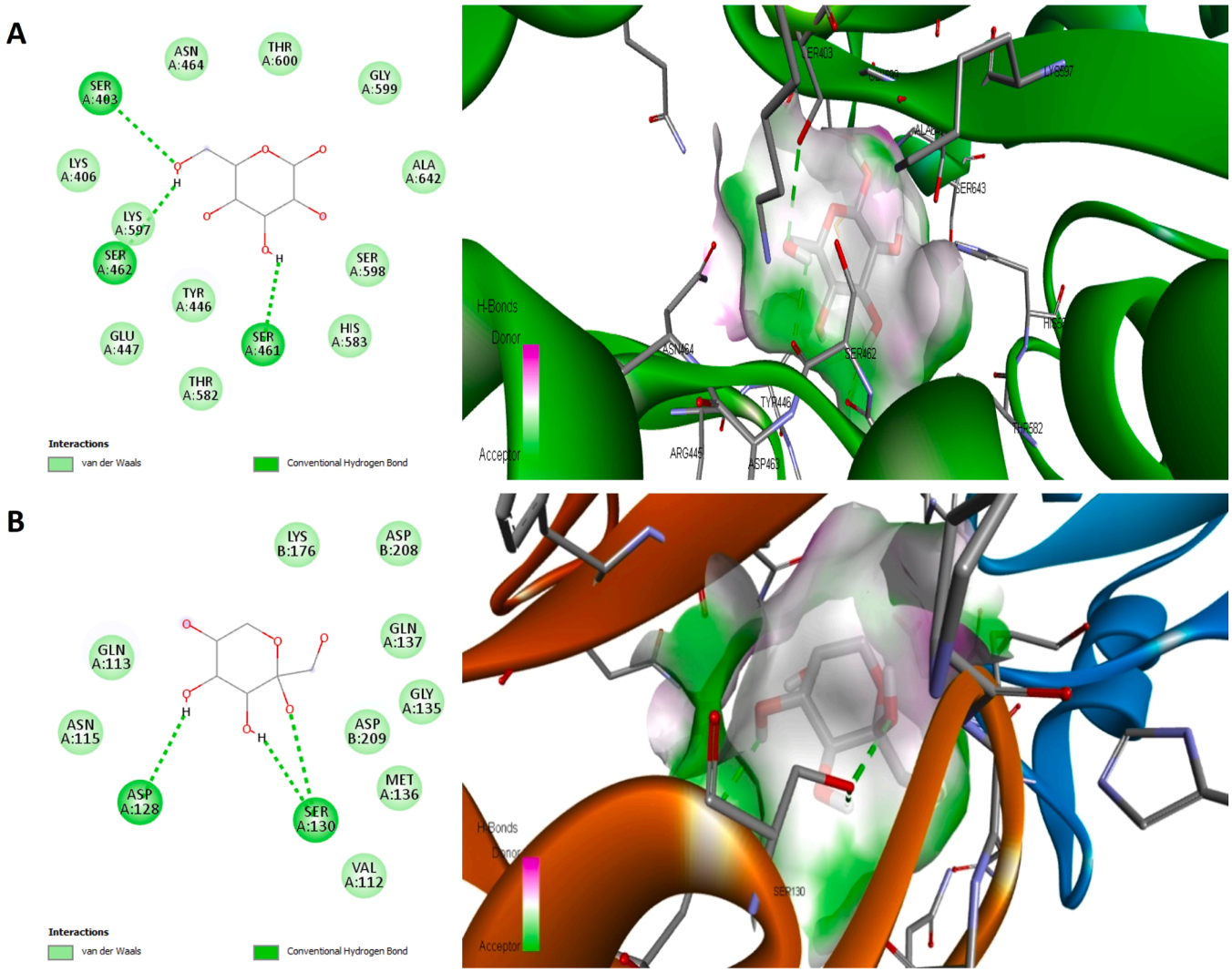

Fig. 14. 2D and 3D structures of D-glucose (a) and D-fructose (b) in PBP2a.

The antibacterial activity data from both well-diffusion and micro-dilution broth assays show a consistent trend. AgNPs synthesized using cottonwood, rambutan, rubber, and coffee honey, which have lower reducing sugar content (Table 1), consistently produce nanoparticles with brighter optical properties (Fig. 5), lower absorbance (Fig. 5), and smaller particle sizes, resulting in superior antibacterial activity.

The antibacterial activity of AgNPs is strongly influenced by their particle size, with smaller particles exhibiting greater efficacy. This finding is further supported by several comparisons from various references listed in Table 4, which consistently demonstrate that AgNP size plays a crucial role in determining their antibacterial activity. In this study, AgNPs synthesized using honey, which resulted in the smallest particle size (9.85 nm), demonstrated the largest inhibition zones against *S. aureus* (14.52 ± 0.36 mm) and *P. aeruginosa* (15.10 ± 0.99 mm). This can be attributed to the larger surface area-to-volume ratio of smaller nanoparticles, which allows for more efficient interactions with bacterial cell membranes, leading to increased cellular uptake and disruption of bacterial functions. Smaller AgNPs release a higher concentration of silver ions, which can cause oxidative stress, protein denaturation, and enzyme inactivation, thereby enhancing their bactericidal properties.

Conversely, AgNPs synthesized via the chemical reduction method using trisodium citrate exhibited negligible antibacterial activity ("slight" inhibition zones for both bacterial strains). This reduced efficacy can be explained by the lack of bioactive compounds in the chemical method, which does not provide the synergistic antimicrobial effect seen with natural reducing agents. Furthermore, chemical synthesis may lead to nanoparticle aggregation, increasing particle size and reducing surface area, thus diminishing the interaction between AgNPs and bacterial cells.

In contrast, bioreductors such as honey, *A. vera*, and *S. polyanthum* offer dual functionality by not only acting as reducing and stabilizing agents but also contributing intrinsic antibacterial properties due to the presence of bioactive compounds like flavonoids, phenolics, and tannins. These compounds act synergistically with AgNPs, enhancing their bactericidal effects. For instance, honey contains phenolic acids and flavonoids, while *Aloe vera* is rich in antimicrobial compounds such as aloin and emodin. Similarly, *S. polyanthum* provides tannins and flavonoids that enhance AgNPs' antibacterial performance. This synergistic interaction between AgNPs and bioactive plant compounds significantly improves the nanoparticles' antimicrobial properties, explaining the superior inhibition zones observed with naturally synthesized AgNPs compared to chemically synthesized ones.

The antibacterial mechanism of AgNPs with a particle size of less than 10 nm (as observed in this research) can be explained through several key stages. These small particles can bind to cell wall components, such as peptidoglycan in Gram-positive bacteria or lipopolysaccharides in Gram-negative bacteria (More et al., 2023). AgNPs of

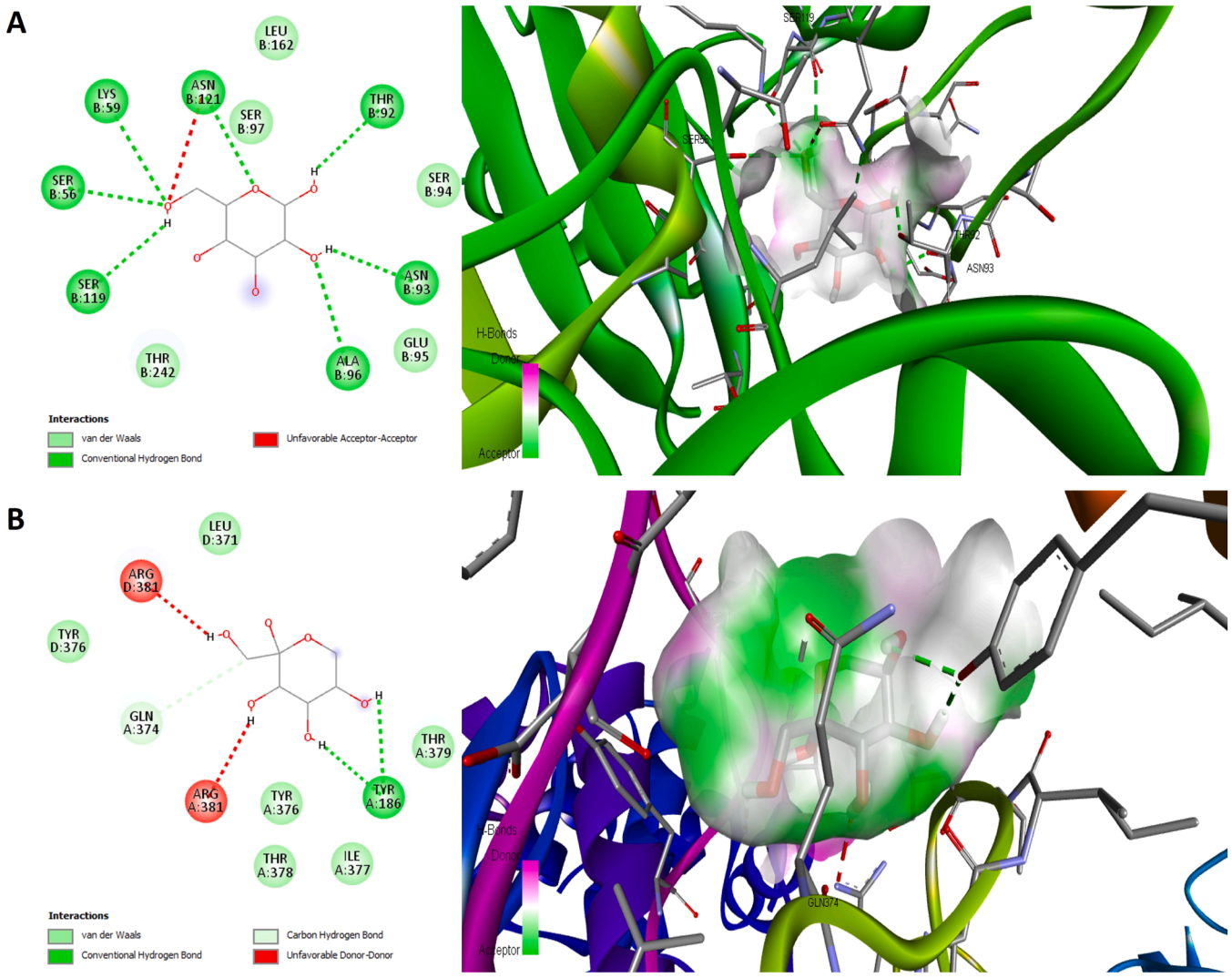

Fig. 15. 2D and 3D structures of D-glucose (a) and D-fructose (b) in PBP3.

approximately 10 nm are sufficiently small to pass through bacterial membrane pores via passive transport. Once inside the cell, these nanoparticles can interact directly with internal components, such as ribosomes, thereby inhibiting protein synthesis. AgNPs within the bacterial cytoplasm can bind to DNA, disrupting genetic replication and potentially causing DNA fragmentation, ultimately leading to cell death (Ahmad et al., 2020). Additionally, AgNPs can induce protein aggregation, impairing essential bacterial protein functions (Shi et al., 2019). Misfolded or structurally disrupted proteins caused by AgNPs may lead to organelle dysfunction and bacterial metabolic disruption (Ajmal, 2023). Some reports suggest that AgNPs can inhibit bacterial respiration by affecting the electron transport chain in the inner membrane, which reduces ATP production and metabolically weakens bacterial cells (Nie et al., 2023). This property of AgNPs contributes to their potential in addressing antimicrobial resistance, as their diverse and highly reactive antibacterial mechanisms can effectively target and damage bacterial cells.

3.5 In-silico study and antibacterial evaluation

Molecular docking is a widely used in silico method to predict interactions between small molecules, drugs, or phytochemicals and target proteins. It simulates their binding processes, offering insights into binding affinities, conformational stability, and interaction mechanisms. Docking results are essential for identifying promising candidates for experimental validation by providing preliminary data on their binding potential to target proteins. In this study, molecular docking was performed to evaluate interactions between honey-derived phytochemicals and key proteins of *S. aureus* and *P. aeruginosa*. Binding affinities were compared with established controls to assess the antibacterial potential of these compounds. Key parameters, including interaction energies, binding modes, and inhibition constants, were analyzed to elucidate their antibacterial properties.

The molecular docking results given for the target protein PBP2a in *S. aureus*, depicted in Fig. 14, indicate that D-glucose and D-fructose have respective binding affinities of −6.1 kcal/mol and −5.7 kcal/mol, lower than the binding affinity of the control compound Ceftaroline at −9.0 kcal/mol. This hence implies that the control compound binds to PBP2a more strongly and forms a more stable complex with it. Yet it still forms the following hydrogen bonds with residues such as SER403, SER462, and SER461, while its van der Waal interactions are formed by LYS406, LYS597, TYR446, GLU447, THR582, HIS583, SER598, ALA642, GLY599, THR600, and ASN464. In the case of D-fructose, this molecule binds to PBP2a via hydrogen bonds formed with ASP128 and SER130, and via van der Waals interactions between the enzyme and GLN113, ASN115, LYS176, ASP208, GLN137, GLY135, ASP209, MET136, and VAL112. While the obtained binding affinities are not as strong as that of the control, the observed interactions will indicate that

D-glucose and D-fructose may still influence PBP2a activity and, hence, also cause an antibacterial effect if combined with other agents.

Regarding the PBP3 target protein (Fig. 15), D-glucose and D-fructose demonstrate binding affinities of −6.3 kcal/mol and −6.0 kcal/mol, which are lower than the binding affinity of the control compound (ceftazidime) at −8.3 kcal/mol. This implies that the control compound has a more robust interaction with PBP3, likely resulting in a more stable inhibition of the protein. However, D-glucose shows promising interactions through hydrogen bonds with residues such as SER119, SER56, LYS59, ASN121, THR92, ASN93, and ALA96, supported by van der Waals forces with THR242, SER97, LEU162, SER94, and GLU95. D-fructose, on the other hand, forms hydrogen bonds with TYR186 and GLN374, with additional stability provided by van der Waals interactions with TYR376, LEU371, THR379, THR378, and ILE377. While the binding affinity of D-glucose and D-fructose is not as strong as the control, their interactions with PBP3 suggest they may still have a role in modulating bacterial cell wall synthesis, making them valuable components in a multi-target antibacterial strategy.

4. Conclusion

This study reveals that the characteristics and antibacterial activity of silver nanoparticles (AgNPs) synthesized using various types of honey as bioreductors are significantly influenced by the reducing sugar content in the honey. Analysis shows that cottonwood honey has the highest reducing sugar content (56.66 %), followed by rambutan honey (49.95 %), rubber honey (44.54 %), and coffee honey (37.56 %). This variation reflects differences in the sugar composition of nectar from different plant sources. Additionally, AgNPs synthesized with honey having higher reducing sugar content show higher UV-Vis absorbance, indicating larger particle sizes and darker colors. FTIR analysis identifies the presence of functional groups such as -OH and C-H from organic compounds in honey that play a role in stabilizing AgNPs, while XRD analysis confirms the FCC crystal structure of silver in the AgNPs. TEM results show an average AgNP size of about 9.85 nm with a tendency towards polydispersity. AgNPs from coffee honey exhibit slightly higher antibacterial activity compared to others. Better antibacterial performance is associated with smaller AgNP sizes (around 8–10 nm), as smaller particles have a higher surface-to-volume ratio, enhancing their interaction with bacterial cell walls. In-silico studies indicate that D-glucose and D-fructose have lower binding affinities for PBP2a and PBP3 compared to controls, but these interactions suggest potential in modulating target protein activity and providing antibacterial effects when combined with other agents. The study concludes that the type of honey affects the characteristics of the resulting AgNPs and that particle size and reducing sugar content in honey play a crucial role in nanoparticle antibacterial activity.

CRediT authorship contribution statement

Aulanni'am: Supervision, Conceptualization. **Moh. Farid Rahman:** Supervision, Conceptualization. **Akhmad Sabarudin:** Visualization, Writing – review & editing, Supervision, Conceptualization, Writing – original draft, Methodology, Funding acquisition. **Saidun Fiddaroini:** Writing – original draft, Validation, Formal analysis. **Kurnia Indu:** Formal analysis. **Luailik Madaniyah:** Writing – original draft. **Suci Amalia:** Conceptualization, Supervision.

Declaration of generative AI and AI-assisted technologies in the writing process

During the preparation of this work, the authors used ChatGPT to enhance the readability of the English language.

Declaration of Competing Interest

Herewith, We, all authors, affirm that we have no known financial conflicts of interest or personal relationships that could have impacted the work presented in this paper.

Acknowledgment

We would like to thank the Faculty of Science, Brawijaya University for the financial support through the Grant, with the numbers: 02172.6/UN10.F0901/B/KS/2024 and 00140.11/UN10.A0501/B/PT.01.03.2/2024 (PDU-UB).

Data statement

All data related to this article are included in this paper.

Data availability

Data will be made available on request.

References

Abdelgadir, A., Adnan, M., Patel, M., Saxena, J., Alam, M.J., Alshahrani, M.M., Singh, R., Sachidanandan, M., Badraoui, R., Siddiqui, A.J., 2024. Probiotic lactobacillus salivarius mediated synthesis of silver nanoparticles (AgNPs-LS): a sustainable approach and multifaceted biomedical application. Heliyon 10 (18), e37987. https://doi.org/10.1016/j.heliyon.2024.e37987.

Ahmad, S.A., Das, S.S., Khatoon, A., Ansari, M.T., Afzal, M., Hasnain, M.S., Nayak, A.K., 2020. Bactericidal activity of silver nanoparticles: a mechanistic review. Mater. Sci. Energy Technol. 3, 756–769. https://doi.org/10.1016/j.mset.2020.09.002.

Ajmal, M.R., 2023. Protein misfolding and aggregation in proteinopathies: causes, mechanism and cellular response. Diseases 11 (1), 30. https://doi.org/10.3390/diseases11010030.

Alarcon, R., Walter, M., Paez, M., Azócar, M.I., 2023. Ostwald ripening and antibacterial activity of silver nanoparticles capped by anti-inflammatory ligands. Nanomaterials 13 (3), 428. https://doi.org/10.3390/nano13030428.

Alharbi, N.S., Alsubhi, N.S., Felimban, A.I., 2022. Green synthesis of silver nanoparticles using medicinal plants: characterization and application. J. Radiat. Res. Appl. Sci. 15 (3), 109–124. https://doi.org/10.1016/j.jrras.2022.06.012.

Al-mehdhar, A.A., Alarjani, K.M., Aldosari, N.S., Alghamdi, M.A., 2024. Antibacterial efficacy of AgNPs synthesized from extract and staphylococcus aureus culture supernatant. J. King Saud. Univ. Sci. 36 (10), 103464. https://doi.org/10.1016/j.jksus.2024.103464.

Amr, M., Abu-Hussien, S.H., Ismail, R., Aboubakr, A., Wael, R., Yasser, M., Hemdan, B., El-Sayed, S.M., Bakry, A., Ebeed, N.M., Elhariry, H., Galal, A., Abd-Elhalim, B.T., 2023. Utilization of biosynthesized silver nanoparticles from agaricus bisporus extract for food safety application: synthesis, characterization, antimicrobial efficacy, and toxicological assessment. Sci. Rep. 13 (1), 15048. https://doi.org/10.1038/s41598-023-42103-3.

Asif, M., Yasmin, R., Asif, R., Ambreen, A., Mustafa, M., Umbreen, S., 2022. Green synthesis of silver nanoparticles (AgNPs), structural characterization, and their antibacterial potential, 155932582210887 Dose Response 20 (2). https://doi.org/10.1177/15593258221088709.

Cianciosi, D., Forbes-Hernández, T., Afrin, S., Gasparrini, M., Reboredo-Rodriguez, P., Manna, P., Zhang, J., Bravo Lamas, L., Martínez Flórez, S., Agudo Toyos, P., Quiles, J., Giampieri, F., Battino, M., 2018. Phenolic compounds in honey and their associated health benefits: a review. Molecules 23 (9), 2322. https://doi.org/10.3390/molecules23092322.

De Leersnyder, I., De Gelder, L., Van Driessche, I., Vermeir, P., 2019. Revealing the importance of aging, environment, size and stabilization mechanisms on the stability of metal nanoparticles: a case study for silver nanoparticles in a minimally defined and complex undefined bacterial growth medium. Nanomaterials 9 (12), 1684. https://doi.org/10.3390/nano9121684.

Dhaka, A., Chand Mali, S., Sharma, S., Trivedi, R., 2023. A review on biological synthesis of silver nanoparticles and their potential applications. Results Chem. 6, 101108. https://doi.org/10.1016/j.rechem.2023.101108.

Fiddaroini, S., Indu, K., Amalia, S., Wulandari, I.O., Mulyasuryani, A., Dinira, L., Sabarudin, A., 2023. Cottonwood honey (Ceiba pentandra) as bioreductor for preparation of AgNPs-mediated Chitosan-based hand gel sanitizer. Trop. J. Nat. Prod. Res. 7 (12). https://doi.org/10.26538/tjnpr/v7i12.29.

Fiddaroini, S., Indu, K., Madaniyah, L., Amalia, S., Aulanni'am, Rahman, Moh F., Sabarudin, A., 2025. Chitosan-Coated silver nanoparticles with various floral honey bioreductors: a promising nonalcoholic hand gel sanitizer formulation. OpenNano 21, 100228. https://doi.org/10.1016/j.onano.2024.100228.

Galatage, S.T., Hebalkar, A.S., Dhobale, S.V., Mali, O.R., Kumbhar, P.S., Nikade, S.V., Killedar, S.G., 2021. Silver nanoparticles: properties, synthesis, characterization, applications and future trends. In: Kumar, S., Kumar, P., Shakher Pathak, C. (Eds.),

Silver Micro-Nanoparticles—Properties, Synthesis, Characterization, and Applications. IntechOpen. https://doi.org/10.5772/intechopen.99173.
Gudkov, S.V., Baimler, I.V., Uvarov, O.V., Smirnova, V.V., Volkov, M.Y., Semenova, A.A., Lisitsyn, A.B., 2020. Influence of the concentration of fe and cu nanoparticles on the dynamics of the size distribution of nanoparticles. Front. Phys. 8, 622551. https://doi.org/10.3389/fphy.2020.622551.
Huq, M.A., Akter, S., 2021. Biosynthesis, characterization and antibacterial application of novel silver nanoparticles against drug resistant pathogenic klebsiella pneumoniae and salmonella enteritidis. Molecules 26 (19), 5996. https://doi.org/10.3390/molecules26195996.
Huq, M.A., Ashrafudoulla, M., Rahman, M.M., Balusamy, S.R., Akter, S., 2022. Green synthesis and potential antibacterial applications of bioactive silver nanoparticles: a review. Polymers 14 (4), 742. https://doi.org/10.3390/polym14040742.
Indana, M.K., Gangapuram, B.R., Dadigala, R., Bandi, R., Guttena, V., 2016. A novel Green synthesis and characterization of silver nanoparticles using gum tragacanth and evaluation of their potential catalytic reduction activities with methylene blue and Congo red dyes. J. Anal. Sci. Technol. 7 (1), 19. https://doi.org/10.1186/s40543-016-0098-1.
Iwuji, C., Saha, H., Ghann, W., Dotson, D., Bhuiya, M.A.K., Parvez, M.S., Jahangir, Z.S., Rahman, M.M., Chowdhury, F.I., Uddin, J., 2024. Synthesis and characterization of silver nanoparticles and their promising antimicrobial effects. Chem. Phys. Impact 9, 100758. https://doi.org/10.1016/j.chphi.2024.100758.
Jassim, A.Y., Wang, J., Chung, K.W., Loosli, F., Chanda, A., Scott, G.I., Baalousha, M., 2022. Comparative assessment of the fate and toxicity of chemically and biologically synthesized silver nanoparticles to juvenile clams. Colloids Surf. B Biointerfaces 209, 112173. https://doi.org/10.1016/j.colsurfb.2021.112173.
Keskin, M., Kaya, G., Bayram, S., Kurek-Górecka, A., Olczyk, P., 2023. Green synthesis, characterization, antioxidant, antibacterial and enzyme inhibition effects of chestnut (Castanea sativa) honey-mediated silver nanoparticles. Molecules 28 (6), 2762. https://doi.org/10.3390/molecules28062762.
Khan, S., Rukayadi, Y., Jaafar, A.H., Ahmad, N.H., 2023. Antibacterial potential of silver nanoparticles (SP-AgNPs) synthesized from syzygium polyanthum (Wight) walp. Against selected foodborne pathogens. Heliyon 9 (12), e22771. https://doi.org/10.1016/j.heliyon.2023.e22771.
Khan, I., Saeed, K., Khan, I., 2019. Nanoparticles: properties, applications and toxicities. Arab. J. Chem. 12 (7), 908–931. https://doi.org/10.1016/j.arabjc.2017.05.011.
Krishnan, P.D., Banas, D., Durai, R.D., Kabanov, D., Hosnedlova, B., Kepinska, M., Fernandez, C., Ruttkay-Nedecky, B., Nguyen, H.V., Farid, A., Sochor, J., Narayanan, V.H.B., Kizek, R., 2020. Silver nanomaterials for wound dressing applications. Pharmaceutics 12 (9), 821. https://doi.org/10.3390/pharmaceutics12090821.
Kumar, A.S., Madhu, G., John, E., Kuttinarayanan, S.V., Nair, S.K., 2020. Optical and antimicrobial properties of silver nanoparticles synthesized via Green route using honey. Green Process. Synth. 9 (1), 268–274. https://doi.org/10.1515/gps-2020-0029.
Kusi, J., Scheuerman, P.R., Maier, K.J., 2020. Antimicrobial properties of silver nanoparticles May interfere with fecal indicator bacteria detection in pathogen impaired streams. Environ. Pollut. 263, 114536. https://doi.org/10.1016/j.envpol.2020.114536.
Lee, S., Jun, B.-H., 2019. Silver nanoparticles: synthesis and application for nanomedicine. Int. J. Mol. Sci. 20 (4), 865. https://doi.org/10.3390/ijms20040865.
Long, Y., Hu, S., Lei, P., Li, Y., 2022. Preparation of Green silver nanoparticles with high antibacterial ability using N-maleoyl chitosan and montmorillonite. Mater. Lett. 316, 132044. https://doi.org/10.1016/j.matlet.2022.132044.
Madaniyah, L., Fiddaroini, S., Hayati, E.K., Rahman, Moh F., Sabarudin, A., 2025b. Stability of biologically synthesized silver nanoparticles (AgNPs) using acalypha indica L. Plant extract as bioreductor and their potential as anticancer agents against T47D cells. Sci. Technol. Indones. 10 (1), 101–110. https://doi.org/10.26554/sti.2025.10.1.101-110.
Madaniyah, L., Fiddaroini, S., Hayati, E.K., Rahman, Moh F., Sabarudin, A., 2025a. Biosynthesis, characterization, and in-vitro anticancer effect of plant-mediated silver nanoparticles using acalypha indica linn: In-silico approach. OpenNano 21, 100220. https://doi.org/10.1016/j.onano.2024.100220.
Mamdouh, S., Mahmoud, A., Samir, A., Mobarak, M., Mohamed, T., 2022. Using femtosecond laser pulses to investigate the nonlinear optical properties of silver nanoparticles colloids in distilled water synthesized by laser ablation. Phys. B Condens. Matter 631, 413727. https://doi.org/10.1016/j.physb.2022.413727.
Mavani, K., Shah, M., 2013. Synthesis of silver nanoparticles by using sodium borohydride as a reducing agent. IJERT. https://doi.org/10.13140/2.1.3116.8648. V2IS3605.
Mikhailova, E.O., 2020. Silver nanoparticles: mechanism of action and probable bio-application. J. Funct. Biomater. 11 (4), 84. https://doi.org/10.3390/jfb11040084.
More, P.R., Pandit, S., Filippis, A.D., Franci, G., Mijakovic, I., Galdiero, M., 2023. Silver nanoparticles: bactericidal and mechanistic approach against drug resistant pathogens. Microorganisms 11 (2), 369. https://doi.org/10.3390/microorganisms11020369.
Naganthran, A., Verasoundarapandian, G., Khalid, F.E., Masarudin, M.J., Zulkharnain, A., Nawawi, N.M., Karim, M., Che Abdullah, C.A., Ahmad, S.A., 2022. Synthesis, characterization and biomedical application of silver nanoparticles. Materials 15 (2), 427. https://doi.org/10.3390/ma15020427.
Nepi, M., Grasso, D.A., Mancuso, S., 2018. Nectar in Plant–Insect mutualistic relationships: from food reward to partner manipulation. Front. Plant Sci. 9, 1063. https://doi.org/10.3389/fpls.2018.01063.
Nicolson, S.W., 2022. Sweet solutions: nectar chemistry and quality. Philos. Trans. R. Soc. B Biol. Sci. 377 (1853), 20210163. https://doi.org/10.1098/rstb.2021.0163.
Nie, P., Zhao, Y., Xu, H., 2023. Synthesis, applications, toxicity and toxicity mechanisms of silver nanoparticles: a review. Ecotoxicol. Environ. Saf. 253, 114636. https://doi.org/10.1016/j.ecoenv.2023.114636.
Obaid, Z.H., Juda, S.A., Kaizal, A.F., Mohammed Salman, J., 2024. Biosynthesis of silver nano particles (AgNPs) from blue Green algae (Arthrospira platensis) and their anti-pathogenic applications. J. King Saud. Univ. Sci. 36 (7), 103264. https://doi.org/10.1016/j.jksus.2024.103264.
Olas, B., 2020. Honey and its phenolic compounds as an effective natural medicine for cardiovascular diseases in humans? Nutrients 12 (2), 283. https://doi.org/10.3390/nu12020283.
Qaeed, M.A., Hendi, A., Obaid, A.S., Thahe, A.A., Osman, A.M., Ismail, A., Mindil, A., Eid, A.A., Aqlan, F., Osman, N.M.A., AL-Farga, A., Al-Maaqar, S.M., Saif, A.A., 2023. The effect of different aqueous solutions ratios of ocimum basilicum utilized in AgNPs synthesis on the inhibition of bacterial growth. Sci. Rep. 13 (1), 5866. https://doi.org/10.1038/s41598-023-31221-7.
Qing, Y., Cheng, L., Li, R., Liu, G., Zhang, Y., Tang, X., Wang, J., Liu, H., Qin, Y., 2018. Potential antibacterial mechanism of silver nanoparticles and the optimization of orthopedic implants by advanced modification technologies. Int. J. Nanomed. 13, 3311–3327. https://doi.org/10.2147/IJN.S165125.
Rai, M., Ingle, A.P., Trzcińska-Wencel, J., Wypij, M., Bonde, S., Yadav, A., Kratošová, G., Golińska, P., 2021. Biogenic silver nanoparticles: what we know and what do we need to know? Nanomaterials 11 (11), 2901. https://doi.org/10.3390/nano11112901.
Samuel, M.S., Ravikumar, M., John, J., A., Selvarajan, E., Patel, H., Chander, P.S., Soundarya, J., Vuppala, S., Balaji, R., Chandrasekar, N., 2022. A review on green synthesis of nanoparticles and their diverse biomedical and environmental applications. Catalysts 12 (5), 459. https://doi.org/10.3390/catal12050459.
Semchyshyn, H.M., Miedzobrodzki, J., Bayliak, M.M., Lozinska, L.M., Homza, B.V., 2014. Fructose compared with glucose is more a potent glycoxidation agent in vitro, but not under carbohydrate-induced stress in vivo: potential role of antioxidant and antiglycation enzymes. Carbohydr. Res. 384, 61–69. https://doi.org/10.1016/j.carres.2013.11.015.
Shi, T., Wei, Q., Wang, Z., Zhang, G., Sun, X., He, Q.-Y., 2019. Photocatalytic protein damage by silver nanoparticles circumvents bacterial stress response and multidrug resistance. mSphere 4 (3), e00175-19. https://doi.org/10.1128/mSphere.00175-19.
Strapasson, G.B., De C. Flach, E., Assis, M., Corrêa, S.A., Longo, E., Machado, G., Santos, J.F.L., Weibel, D.E., 2023. Eco-friendly synthesis of silver nanoparticles and its application in hydrogen photogeneration and nanoplasmonic biosensing. ChemPhysChem 24 (21), e202300002. https://doi.org/10.1002/cphc.202300002.
Sun, H., Jiao, R., Xu, H., An, G., Wang, D., 2019. The influence of particle size and concentration combined with ph on coagulation mechanisms. J. Environ. Sci. 82, 39–46. https://doi.org/10.1016/j.jes.2019.02.021.
Thanh, N.T.K., Maclean, N., Mahiddine, S., 2014. Mechanisms of nucleation and growth of nanoparticles in solution. Chem. Rev. 114 (15), 7610–7630. https://doi.org/10.1021/cr400544s.
Tiwari, H., Samal, K., Geed, S.R., Bera, S., Das, C., Mohanty, K., 2023. Green synthesis of silver nanoparticles for ultrafiltration membrane surface modification and antimicrobial activity. Sustain. Chem. Clim. Action 3, 100031. https://doi.org/10.1016/j.scca.2023.100031.
Yahia, E.M., Carrillo-López, A., Bello-Perez, L.A., 2019. Carbohydrates. Postharvest Physiology and Biochemistry of Fruits and Vegetables. Elsevier, pp. 175–205. https://doi.org/10.1016/B978-0-12-813278-4.00009-9.
Yang, F., 2021. Diffusion-Limited growth of a spherical nanocrystal in a finite space. Langmuir 37 (13), 3912–3921. https://doi.org/10.1021/acs.langmuir.1c00140.
Yudaev, P., Mezhuev, Y., Chistyakov, E., 2022. Nanoparticle-containing wound dressing: antimicrobial and healing effects. Gels 8 (6), 329. https://doi.org/10.3390/gels8060329.
Zhang, Z., Lan, X., Wen, G., Long, Q., Yang, X., 2021. An experimental study on the particle size and shape distribution of coal drill cuttings by dynamic image analysis. Geofluids 2021, 1–11. https://doi.org/10.1155/2021/5588248.
Zielińska, A., Skwarek, E., Zaleska, A., Gazda, M., Hupka, J., 2009. Preparation of silver nanoparticles with controlled particle size. Procedia Chem. 1 (2), 1560–1566. https://doi.org/10.1016/j.proche.2009.11.004.